Science Translational Medicine AAAS

Submitted Manuscript: Confidential template updated: February 28 2012

CPEB alteration and aberrant transcriptome-polyadenylation unveil a treatable SLC19A3 deficiency in Huntington's disease

Authors: Sara Picó[1,2†], Alberto Parras[1,2†], María Santos-Galindo[1,2], Julia Pose-Utrilla[2,3], Margarita Castro[1,4,5], Enrique Fraga[1,2], Ivó H. Hernández[1,2,6], Ainara Elorza[1,2], Héctor Anta[7,8], Nan Wang[9], Laura Martí-Sánchez[5,10], Eulàlia Belloc[8], Paula García-Esparcia[2,11], Juan J. Garrido[2,12], Isidro Ferrer[2,11], Daniel Macías-García[2,13], Pablo Mir[2,13], Rafael Artuch[5,10], Belén Pérez[1,4,5], Félix Hernández[1,2], Pilar Navarro[7,14], José Luis López-Sendón[15], Teresa Iglesias[2,3], X. William Yang[9], Raúl Méndez[8,16] and José J. Lucas[1,2]*

Affiliations:
[1]Center for Molecular Biology "Severo Ochoa" (CBMSO) CSIC/UAM, Madrid 28049, Spain.
[2]Networking Research Center on Neurodegenerative Diseases (CIBERNED). Instituto de Salud Carlos III, Madrid, Spain.
[3]Instituto de Investigaciones Biomédicas "Alberto Sols", Consejo Superior de Investigaciones Científicas-Universidad Autónoma de Madrid (CSIC-UAM), Madrid, Spain.
[4]Centro de Diagnóstico de Enfermedades Moleculares (CEDEM), Madrid 28049, Spain.
[5]Centro de Investigación Biomédica en Red de Enfermedades Raras (CIBERER), ISCIII, Madrid, Spain.
[6]Facultad de Ciencias, Departamento de Biología (Unidad Docente Fisiología Animal), Universidad Autónoma de Madrid, Madrid 28049, Spain.
[7] Cancer Research Program, Hospital del Mar Medical Research Institute (IMIM), Unidad Asociada I+D+i IMIM-IIBB (CSIC), Barcelona, Spain.
[8]Institute for Research in Biomedicine (IRB), Barcelona Institute of Science and Technology, 08028 Barcelona, Spain.
[9]Center for Neurobehavioral Genetics, Jane and Terry Semel Institute for Neuroscience and Human Behavior; Department of Psychiatry and Biobehavioral Sciences; Brain Research Institute, David Geffen School of Medicine at UCLA, Los Angeles, CA, 90095, USA.
[10]Department of Clinical Biochemistry, Institut de Recerca Sant Joan de Déu, Barcelona, Spain.
[11]Institute of Neuropathology; IDIBELL-University Hospital Bellvitge; University of Barcelona; Hospitalet de Llobregat; Barcelona 08908, Spain.
[12]Department of Molecular, Cellular and Developmental Neurobiology, Instituto Cajal (CSIC), Madrid, Spain.
[13]Unidad de Trastornos del Movimiento, Servicio de Neurología y Neurofisiología Clínica, Instituto de Biomedicina de Sevilla (IBiS), Hospital Universitario Virgen del Rocío/CSIC/Universidad de Sevilla, Sevilla 41013, Spain.
[14]Institute of Biomedical Research of Barcelona (IIBB-CSIC), Barcelona, Spain.
[15]Department of Neurology, Hospital Ramón y Cajal, Instituto Ramón y Cajal de Investigación Sanitaria (IRYCIS), Madrid 28034, Spain.
[16]Institució Catalana de Recerca i Estudis Avançats (ICREA), Barcelona 08010, Spain.

*To whom correspondence should be addressed:
José J. Lucas
jjlucas@cbm.csic.es
Center for Molecular Biology-Severo Ochoa (CBMSO)
C/ Nicolás Cabrera,1. 28049 Madrid. Spain
Tel. +34 91 196 4552
http://www.cbm.uam.es/LucasLab

† These authors contributed equally

One Sentence Summary: Altered CPEBs and mRNA-poly(A) unveil a BTBGD-like thiamine deficiency in HD

Abstract

Huntington's disease (HD) is a devastating hereditary neurodegenerative disorder of the basal ganglia for which disease-modifying treatments are not available. Although promising gene-silencing therapies are currently being tested, new molecular mechanisms underneath the triggering mutation must be explored to identify easily druggable targets. Cytoplasmic polyadenylation element binding proteins 1–4 (CPEB1–4) are RNA-binding proteins that repress or activate translation of CPE-containing transcripts by, respectively, shortening or elongating their poly(A) tail. Here we report increased CPEB1 and decreased CPEB4 protein levels in striatum of HD patients and mouse models. This correlates with a reprogramming of polyadenylation in 17.3% of the transcriptome that markedly affects neurodegeneration-associated genes (like *PSEN1, MAPT, SNCA, LRRK2, PINK1, DJ1, SOD1, TARDBP, FUS* and *HTT*), thus suggesting a new molecular mechanism in neurodegenerative disease aetiology. Besides, we found decreased protein levels of top deadenylated transcript-genes which include striatal atrophy-linked genes not previously related to HD such as *KTN1* and, remarkably, the easily druggable *SLC19A3* (ThTr2 thiamine transporter). Mutations in *SLC19A3* cause biotin-thiamine-responsive basal ganglia disease (BTBGD), a devastating striatal disorder that however reverts upon a vitamin-based therapy. Decreased ThTr2 in HD led to discover that, alike BTBGD patients, HD patients show decreased CSF thiamine levels. Furthermore, HD patients and mice show decreased striatal concentrations of TPP, the metabolically active form of thiamine. Remarkably, a high dose biotin+thiamine treatment used to revert BTBGD prevented the TPP deficiency of HD mice and attenuated their radiological, neuropathological and motor HD-like phenotypes, thus unveiling an easy to implement therapy for HD.

Introduction

Huntington's disease (HD) is a devastating hereditary neurodegenerative disorder characterized by atrophy of the basal ganglia, particularly the striatum, and prominent motor symptoms (*1*). The underlying mutation is an expanded CAG repeat in the *Huntingtin* (*HTT*) gene, which codes for a self-aggregating polyglutamine (polyQ) tract in the N-terminal region of the protein (*1*). Although HTT lowering strategies currently in clinical trials are promising therapeutic strategies (*2*), they may be challenged by limitations associated to efficacy of delivery to the basal ganglia and side effect issues (*3*). It is therefore important to keep elucidating the molecular mechanisms by which the triggering mutation elicits its toxicity as a way to find easily druggable targets.

Similar polyQ-encoding CAG mutations in different genes cause spinal-bulbar muscular atrophy (SBMA), dentatorubral-pallidoluysian atrophy (DRPLA) and multiple dominant spinocerebellar ataxias (SCAs) such as SCA-1, -2, -3, -6, -7 or -17 (*4*) and there is evidence of toxicity being mediated by both the expanded CAG-containing mRNAs and the polyQ-containing proteins (*5, 6*). Interestingly, one of the few genes able to act as a dual modifier of the toxicities induced by either CAG-repeat mRNA or polyQ in *Drosophila* models of SCA-3 is *Orb2* (*6*), the orthologue of mammalian *CPEB2-4*.

Cytoplasmic polyadenylation element binding proteins 1–4 (CPEB1–4) are RNA binding proteins that recognize transcripts that harbor CPE sequences in their 3'UTR -approximately 40% of the transcriptome (*7, 8*)- and that repress or activate their translation by inducing shortening or elongation of their poly(A) tail (*9*). This CPEB-dependent regulation of transcriptome polyadenylation occurs in the cytoplasm and confers an additional layer of post-transcriptional

regulation of gene expression (*9, 10*). CPEBs play a key role in early development (*9*) and they also act in adult neurons to enable synaptic plasticity through prion-like mechanisms (*9, 11*).

Altered CPEBs and subsequent alteration in transcriptome polyadenylation have been associated to the aetiology of various diseases such as cancer (*12, 13*), chronic liver disease (*14*), epilepsy (*15*) or autism (*8*), thus leading to the identification of new possible therapeutic targets among CPEB-dependent dysregulated genes. However, a potential role of CPEBs in neurodegenerative disorders has not been fully explored.

Interestingly, we noticed that HD-related genes are prevalent among genes that are mistranslated in the absence of CPEB1 (*16*). This, together with the mentioned ability of CPEBs to modulate CAG/PolyQ toxicity in flies (*6*), led us to characterize the status of CPEBs and of global mRNA-polyadenylation in HD as a way to deepen on the molecular pathogenesis of HD and to explore new possible therapeutic targets.

Results

CPEB1/4 imbalance in HD striatum

To explore the status of CPEBs in HD we performed Western blot analysis on post-mortem striatal tissue from HD cases and control subjects. This revealed markedly increased CPEB1 (303%, $P=6\times10^{-3}$) and markedly decreased CPEB4 (51%, $P=1.4\times10^{-5}$) protein levels in HD striatum (Fig. 1A), while no significant changes were observed regarding CPEB2 or CPEB3 (fig. S1A). We then explored whether a similar alteration of CPEBs takes place in mouse models of HD. We first analysed the widely used R6/1 mouse model which overexpresses exon1-mutant *Htt* thus resulting in a robust, yet slowly-progressing, motor phenotype. Similar to human samples, striatal homogenates from R6/1 mice showed increased CPEB1 and decreased CPEB4 protein levels (Fig.

1B) without changes in CPEB2 or CPEB3 (fig. S1B). Next, we analysed zQ175 mice, a heterozygous knock-in HD model with CAG expansion in the endogenous *Htt* gene which better resembles the human HD mutation, but that does not develop an overt motor phenotype within the maximal (approximately 2.5 years) lifespan of a mouse. In this model of pre-manifest HD, we only observed the decrease in striatal CPEB4 protein levels (fig. S1C) thus suggesting that the decrease in CPEB4 levels observed in HD patients and R6/1 mice precedes the increase in CPEB1.

To test whether the marked CPEB1/CPEB4 protein imbalance in symptomatic HD patients and mice is due to matching changes at transcript level, we then performed RT-PCR analysis (fig. S1, D and E). Regarding CPEB1, we observed a tendency to increased transcript level in human HD striatum and a significant increase in R6/1 striatum that might account for the increased CPEB1 protein levels. Regarding CPEB4, mRNA levels were unaltered in HD and R6/1 striatum, thus suggesting that the observed decreased CPEB4 protein levels are likely due to posttranscriptional mechanisms. In this regard, and given the ability of CPEBs to act as physiological prions (*11, 17*), we performed immunohistochemistry of CPEB4 in R6/1 mice to test whether the decrease in soluble CPEB4 was due to sequestration into the characteristic nuclear inclusion bodies. However, R6/1 mice showed homogeneous decrease of the cytoplasmic neuronal CPEB4 staining (Fig. 1C) without co-localization with the Htt-positive intranuclear inclusions (Fig. 1D). In summary, these results demonstrate that CPEBs are altered in HD with CPEB1 being increased and CPEB4 decreased in striatum of symptomatic HD patients and mice.

CPEB4 overexpression attenuates HD-like motor phenotype

To explore whether the observed alterations in CPEBs are likely contributors to HD pathogenesis, we decided to perform mouse genetics analysis. For this, we took advantage of previously

generated CPEB1-deficient (CPEB1 heterozygous KO, CPEB1$^{+/-}$) (*14*) and CPEB4 overexpressing (CamkII-tTA:TRE-CPEB4, TgCPEB4) (*8*) mice. These mice were bred with R6/1 mice to test whether attenuation of the excess CPEB1 or of the decreased CPEB4, results in amelioration of the R6/1 HD-like motor phenotype. We found that R6/1:CPEB1$^{+/-}$ mice perform very similar to R6/1 mice in the tests that detect HD-associated impaired motor coordination and hypolocomotion, the rota-rod and the open field tests, respectively (Fig. 2, A and B). The R6/1:CPEB1$^{+/-}$ mice even show a tendency to worse performance in the inverted grid test that detects deficits in limb strength (Fig. 2C). Regarding CPEB4 overexpressing mice, R6/1:TgCPEB4 mice show a significant attenuation of the motor coordination deficit observed in the rotarod (Fig. 2D) and a tendency to less hypoactivity in the open field, as compared to R6/1 mice (Fig. 2E). A slight tendency to better performance in the inverted grid test was also observed for R6/1:TgCPEB4 mice (Fig. 2F). Altogether, and in good agreement with the ability of Orb2 to act as a modifier of CAG/polyQ toxicity in fly models (*6*), these results indicate that CPEB-alteration, particularly the decrease in CPEB4, contributes to HD pathogenesis.

Altered transcriptome polyadenylation affects genes linked to major neurodegenerative diseases

We then tested whether the CPEB-alteration observed in striatum of HD patients and mice correlates with changes in transcriptome polyadenylation. For this, we extracted total RNA from striatum of R6/1 and wild type mice and performed poly(U) chromatography followed by gene chip analysis. This revealed that in R6/1 striatum, transcript poly(A) tail length increased in 8.7%, and decreased in 8.6%, of the analysed genes (Fig. 3A; table S1A). Interestingly, we performed gene ontology analysis (using KEGG pathways) of the 1,467 genes with absolute poly(A) fold-change (FC) above 2 and found that the three terms with significant Benjamini–Hochberg

corrected *P*-value were: HD, Alzheimer's disease (AD) and Parkinson's disease (PD) (Fig. 3B; table S1B). Thus suggesting that altered polyadenylation may contribute to pathogenesis not only in HD but also across the main neurodegenerative disorders. In good agreement with this, genes playing key roles in neurodegeneration—such as those mutated in familial forms of AD/tauopathies, PD or amyotrophic lateral sclerosis (including *PSEN1, MAPT, SNCA, LRRK2, PINK1, DJ1, SOD1, TARDBP, FUS*) and *HTT* itself—showed altered polyadenylation (Fig. 3C and table S1A). Interestingly, this may explain why some of the neurodegeneration-related genes, such as *MAPT* and *GSK3B*, have been reported to display detrimental altered protein levels in brains of HD patients and mice without matching alterations at the transcript level (*18, 19*). In summary, we have found that the striatum of symptomatic HD mice shows an alteration of poly(A) tail length in 17.3% of the transcriptome that markedly affects neurodegeneration associated genes, thus suggesting a new molecular mechanism in the aetiology of HD and possible also in other major neurodegenerative diseases.

Top deadenylated genes include striatal atrophy-linked genes and show decreased protein levels

Interestingly, we analysed the presence of CPE sequences in the UTR of the genes showing altered polyadenylation and we observed an enrichment selectively in the genes showing deadenylation (Fig. 4A). Strikingly, among the most markedly deadenylated genes (FC <–4.0), the percentage of CPE-containing genes was 93% (Fig. 4B). Shortening of the poly(A) tail is associated to diminished translation and decreased protein levels (*20*), thus suggesting a possible CPEB-dependent decrease in protein levels of deadenylated transcripts. In fact, we confirmed reduced protein levels of top deadenylated genes such as AUTS2, ROCK1 and KTN1 both in HD and R6/1 striatal tissue, despite unaltered transcript levels (Fig. 4, B and C). Remarkably, decreased KTN1

protein levels may be relevant to the striatal atrophy in HD, as a genome-wide association study of common variants affecting volume of subcortical regions revealed that the size of the striatum is proportional to *KTN1* gene expression (*21*). Also among these top deadenylated (FC <–4) genes, extremely interesting regarding both potential causative role in striatal degeneration and therapeutic relevance for HD was *SLC19A3* (Fig. 4B), because its mutation causes biotin-thiamine-responsive basal ganglia disease (BTBGD; OMIM #607483), a devastating neural disorder with prominent striatal affectation that can however be reverted with a vitamin-based therapy (*22*, *23*).

HD is a BTBGD-like thiamine deficiency

SLC19A3 encodes the transmembrane thiamine transporter 2 (ThTr2) (*24*). Thiamine (vitamin B1) is a cofactor for multiple enzymes in the catabolism of sugars (*23*). Free thiamine from the diet is converted in cells to its derivatives, thiamine monophosphate (TMP) and thiamine pyrophosphate (TPP) (*23*). TPP is the bioactive form, acting as an enzyme cofactor (*23*). Individuals with BTBGD have decreased cerebrospinal fluid (CSF) thiamine levels despite normal thiamine levels in blood (*25*, *26*), bilateral atrophy in the head of the caudate nucleus and of the putamen as well as a variety of neurological symptoms, including lethargy, irritability, dystonia, spasticity, tremor and chorea, among others. All these symptoms improve upon administration of thiamine (*27*) to compensate for its decreased transporter and biotin (*27*) which is believed to increase *SLC19A3* transcription (*28*, *29*). We therefore hypothesized that HD disease might in part be a phenocopy of BTBGD due to a decrease in ThTR2 protein levels. This might therefore provide a new mechanistic clue about HD as well as a potential novel therapy.

Indeed, we next confirmed by Western blot a marked decrease in ThTr2 levels in both striatum and cortex of individuals with HD despite a tendency to increased transcript levels (Fig.

5A). This was mirrored by strongly decreased staining of the protein by immunohistochemistry in both striatum and cortex, which, in good agreement with the human protein atlas (proteinatlas.org), revealed neuronal and endothelial localization (Fig. 5B). More importantly, in the CSF of individuals with HD, we observed decreased levels of TMP (the prevailing form of thiamine in CSF), despite unaltered blood levels of thiamines (Fig. 5C), thus resembling what has been reported for individuals with BTBGD (*25, 26*). In brain tissue, the cofactor TPP is the predominant form of thiamine (*30*) and it is assumed that CSF thiamine deficiency in BTBGD patients correlates with decreased brain levels of the intracellular cofactor, ultimately leading to neuronal dysfunction. To our knowledge, no data on brain TPP levels are available regarding BTBGD patients. However, we were able to test this in post-mortem samples of HD striatum. Strikingly, we found a marked decrease in TPP concentrations in HD striatal tissue (Fig. 5D). Altogether, these results demonstrate a thiamine deficiency in HD brain and suggest that individuals with HD might benefit from thiamine and/or biotin supplementation therapy, as is seen for individuals with BTBGD.

High biotin+thiamine improves radiology, neuropathology and motor phenotype of HD mice

In order to pre-clinically test the potential of vitamin supplementation for HD, we first confirmed that HD mice also show decreased ThTr2 levels. In the mouse, *Slc19a3* transcript expression is essentially restricted to brain endothelium (vastdb.crg.eu), and we observed that ThTr2 protein was almost absent from the brain vessels isolated from R6/1 mice (fig. S2A) and markedly reduced in those from zQ175 mice (fig. S2B). We then tested whether HD mice also show reduced striatal concentration of TPP and, importantly, whether this would revert upon a regime of high dose biotin and thiamine treatment like the one used in BTBGD patients. We found that both zQ175 and R6/1

mice do show decreased striatal concentration of TPP (Fig. 6, A and B). Importantly, we found that the combined therapy of biotin and thiamine in the drinking water (B+T, see Methods) prevented the decreased striatal content of TPP in both zQ175 and R6/1 mice (Fig. 6, A and B).

As mentioned, symptoms of individuals with BTBGD ameliorate with high doses of biotin considerably exceeding the adequate intake needs (*27, 31*) -presumably through increased *SLC19A3* transcription (*28, 29*)-, with thiamine supplementation, and with combinations of both (*27*). Thus, we tested whether the B+T treatment that normalizes TPP levels in striatum of HD mice was also able to improve their HD-like phenotypes. Although zQ175 mice do not show an overt motor phenotype, they do display striatal atrophy and phosphocreatine spectroscopy alteration (*32*). We performed magnetic resonance imaging (MRI) on untreated 17-week old zQ175 mice to verify striatal atrophy (Fig. 6C) and on treated and untreated 24-week old zQ175 mice to test the possible efficacy of B+T treatment on the striatal atrophy. We found that the B+T treatment prevented the additional striatal atrophy experienced by untreated zQ175 mice and it even showed a tendency to slightly revert the decrease in striatal volume observed in untreated 17 week-old zQ175 mice (Fig. 6D). Similarly, the increase in striatal phosphocreatine signal seen in zQ175 mice by magnetic resonance spectroscopy (MRS), was prevented by B+T treatment (Fig. 6E).

We then tested the effect of B+T treatment on the overt motor phenotype and neuropathology of R6/1 mice. We found that the motor coordination deficit detected with the rotarod test in 13 week- and 18 week-old R6/1 mice was prevented by the B+T treatment (Fig. 6F). Similarly, the deficit in limb strength detected in the inverted grid test at the ages of 18 and 23 weeks was also prevented by the B+T treatment (Fig. 6G). Finally, we measured the striatal area and number of apoptotic (cleaved-caspase 3-positive) neurons in coronal sections of 4.5

month-old R6/1 mice and found that the B+T treatment prevented both the striatal atrophy (Fig. 6H) and the increased number of apoptotic neurons (Fig. 6I). Together, these results, demonstrated that a B+T treatment similar to the one that ameliorates BTBGD patients is able to prevent the brain thiamine deficiency observed in HD mice and to attenuate their radiological, neuropathological and motor HD-like phenotypes, thus evidencing that HD patients might benefit from biotin and thiamine supplementation therapy, as BTBGD patients do.

Discussion

By analysing the status of CPEBs and of global transcriptome polyadenylation in brains of HD patients and mouse models, here we report a pathogenic decrease of CPEB4 as well as an increase in CPEB1 protein levels that correlate with altered polyadenylation of neurodegeneration linked genes, thus unveiling a new molecular mechanism in neurodegenerative disease. Besides, Western blot analysis of CPE-containing deadenylated transcripts allowed us to identify new key striatal atrophy effector genes such as KTN1 and, more importantly, SLC19A3. The latter led us to discover that HD is in part a thiamine deficiency disorder similar to BTBGD, thus unveiling an easy to implement vitamin-based therapy for HD, as evidenced by the also reported behavioural and neuroanatomical improvement of HD mice upon biotin and thiamine supplementation.

HTT gene silencing strategies were pre-clinically proven effective in animal models (*33-35*) and this led to the development of therapies designed to lower *HTT* gene expression in HD patients that are currently in clinical trials (*36, 37*) and that are very attractive because they target the root cause of the disease. However, such HTT-lowering gene therapies may encounter difficulties associated to invasive modes of delivery -often requiring repeated dosage- and to limited coverage of the CNS, among others (*3*). It is therefore important to keep in mind that there

is currently no disease modifying therapy for HD. In this context, the main implication of our study is that it unveils a trivial therapy that is expected to ameliorate the course of the disease and that deserves soon clinical testing.

That biotin and thiamine supplementation may ameliorate the course of the disease in HD patients is evidenced by the fact that we have demonstrated that HD is a BTBGD-like brain thiamine deficit in which the underlying ThTr2 deficiency is caused by decreased *SLC19A3* expression (instead of the *SLC19A3* inactivating mutations that cause BTBGD). Since BTBGD patients recover upon early biotin and thiamine supplementation, HD patients should also improve, particularly if treated early enough. However, although correcting this undoubtedly-pathogenic thiamine deficiency is expected to delay the course of the disease -as seen in R6/1 mice-, we should keep in mind that other aspects of the toxicity triggered by expanded CAG-repeat RNA and/or expanded polyQ will not be solved. In any case, given the parallelism with BTBGD, the combined biotin and thiamine therapy is expected to significantly improve quality of life of patients for some time.

Importantly, the biotin and thiamine supplementation therapy has multiple advantages such as safety and full accessibility to CNS. Regarding safety, both biotin and thiamine are natural vitamins and, accordingly, they are considered nutraceuticals which are FDA-approved, even at high doses in the case of thiamine (https://ods.od.nih.gov/). Besides, safety of the combined high dose of both vitamins has already been reported for BTBGD patients (*27*). Another advantage of this therapy is its low cost. This, together with easy over-the-counter accessibility, may however become a double edge sword at the time of clinical testing. Placebo controlled double bind clinical trials should be efficiently launched in the short term to prevent self-prescription to obscure interpretation of clinical trials, including those aiming to test other therapeutic agents. Government

and non-profit organizations may be key to enable efficient clinical testing of this low cost therapy. Still, the patented use of the specific combined therapy for HD may also make it attractive for pharmaceutical companies.

Apart from SLC19A3, this study may lead to the identification of additional therapeutic targets, such as those that are expected to be mechanistically upstream. Correlative evidence, including the observed phenotypic improvement of mice upon transgenic overexpression of CPEB4, strongly suggests that alteration of CPEBs -and remarkably the decreased CPEB4-, leads to aberrant polyadenylation and subsequent altered protein levels of numerous aetiology-relevant genes. Then, theoretically, therapeutic strategies aimed to correct the decreased CPEB4 protein levels might lead to amendment of pathogenic gene mis-expression globally. However, actual demonstration of the mentioned mechanistic causality is beyond the scope of this study and, besides, the pharmacological modulation of CPEB activity is a challenging issue, particularly to counteract decreased levels and/or activity. Therefore, at this point, therapeutic strategies aiming to increase CPEB4 levels and/or activity do not seem realistic. A more efficient strategy to identify additional therapeutic targets from this study would be to perform a systematic screening of all the neurodegeneration-associated deadenylated transcripts to see which ones are easily druggable to then verify altered proteins levels in HD patients and mouse model tissue prior to preclinical testing in mouse models, similar to what we have already done for SLC19A3.

In summary, this study reveals that alteration of CPEBs and of global mRNA polyadenylation emerges as a new possible molecular mechanism in neurodegeneration. Most importantly, this study has pinpointed diminished ThTr2 levels as a key pathogenic effector and unveiled a brain thiamine deficiency in HD patients, thus evidencing that vitamin supplementation regimes similar to those that benefit BTBGD patients should be given to individuals with HD.

Materials and Methods

Study design. The objectives of this controlled laboratory study were (i) investigate the CPEB and polyadenylation status in HD and HD mice, (ii) analyse global mRNA polyadenylation in HD using the R6/1 mice HD model, (iii) study the status of SLC19A3 and thiamine in HD and (iv) determine whether biotin+thiamine treatment would alleviate HD pathology in HD mouse models. Sample size was determined by availability and previous experience with biochemical and behavioural experiments in the mouse model. A minimum of three individuals (human/mice) per group were used for studies involving statistical analyses, and the n for individual experiments is indicated in the figures. Treated/no-treated mice (see Mouse biotin and thiamine treatments) were randomly allocated to experimental and control groups at weaning. Blinding was performed during data collection and analysis. Outliers were excluded using SPSS 26.0 (see Data analysis). For all human studies, sampling was approved by the local ethics committee, and all subjects signed informed consent. For mouse studies, all experiments were performed according to the guidelines of the Animal Ethics Committee and were approved by the government authorities.

Human tissue samples. Human tissue samples used in immunoblot and immunohistochemistry (IHC) were provided by the Institute of Neuropathology Brain Bank (HUBICO-IDIBELL, Hospitalet de Llobregat, Spain), the Neurological Tissue Bank of the IDIBAPS Biobank (Barcelona, Spain), the Banco de Tejidos Fundación Cien (BT-CIEN, Madrid, Spain) and the Netherlands Brain Bank (Amsterdam, The Netherlands). Written informed consent for brain removal after death for diagnostic and research purposes was obtained from brain donors and/or next of kin.

Cerebrospinal fluids (CSF) were collected in sterile tubes. Total blood was collected in K2E (EDTA) tubes (368801, BD Biosciences). CSF and blood were collected according to Hospital Universitario Ramón y Cajal (Madrid, Spain), Hospital Universitario Virgen del Rocío (Sevilla, Spain) and HUVR-IBiS Biobank (Andalusian Public Health System Biobank and ISCIII-Red de Biobancos PT13/0010/0056) guidelines.

Animals. Different mouse models were used, which have been previously reported: R6/1 transgenic mice for the human exon-1-*Htt* gene (*38*) in B6CBAF1 background, heterozygous knock-in of an expanded CAG track in exon 1 of huntingtin gene, zQ175 mice (*32*) in C57BL/6J background, CPEB1-deficient mice (CPEB1 heterozygous KO, CPEB1+/-) (*14*) in C57BL/6J background and CPEB4 overexpressing mice (CamkII-tTA:TRE-CPEB4, TgCPEB4) (*8*) in C57BL/6J background. All mice were housed in CBMSO animal facility, with four per cage. Food and water were available *ad libitum*, and mice were maintained in a temperature-controlled environment on a 12/12 h light-dark cycle with light onset at 08:00. Thiamine content in chow diet was 7 mg/kg of food pellets, according to the manufacturer (SAFE 150, from Safe-diets, France). Animal housing and maintenance protocols followed the local authority guidelines. Animal experiments were performed under protocols approved by the CBMSO Institutional Animal Care and Utilization Committee (Comité de Ética de Experimentación Animal del CBMSO, CEEA-CBMSO), and Comunidad de Madrid PROEX 293/15.

Mouse biotin and thiamine treatments. Treatment based on thiamine and/or biotin was administered orally in the drinking water, serving as a control of treatment mice with normal drinking water and as a control of genotype non-transgenic litter siblings.

In R6/1 mice, treatment began at 3 weeks of age, just after weaning. Biotin-only treatment consisted of a dose of 10 mg/kg/day; thiamine-only treatment started at a dose of 200 mg/kg/day,

which was decreased to 50 mg/kg/day from 18 weeks; and combined biotin and thiamine (B+T) treatment consisted of a dose of 5 mg/kg/day of biotin + 100 mg/kg/day thiamine, which was reduced to 25 mg/kg/day at the age of 18 weeks. The reason for decreasing thiamine doses from week 18 is that in a pilot group of mice in which the dose was not reduced, a possible toxicity in R6/1 mice was detected from 24 weeks of age, evidenced by an increase in the volume of drink consumed and of urination. These effects were not observed if thiamine concentrations were reduced to a quarter of the initial concentration. Biotin-only and thiamine-only treatments were analysed in the pilot experiment, and no attenuation of the phenotype was observed in the motor coordination test (Rotarod) or in the locomotor activity test (Open Field) (data not shown). In the case of zQ175 mice, B+T treatment consisted of 5 mg/kg/day biotin + 100 mg/kg/day thiamine. The number of animals included in each group is indicated in the results section.

Gene ontology analysis. Transcripts with changes in their poly(A) tail length in St of symptomatic R6/1 mice (FC $\leq$ -2 or $\geq$ 2) were analysed with DAVID Bioinformatics Resources 6.7, KEGG pathway annotation (*39*).

Analysis of CPE sequences. 3'UTR (untranslated region) sequences from selected gene sets were extracted from Ensembl (http://www.ensembl.org/) and incidence of canonical and functional CPE (cytoplasmic polyadenylation element) sequences was detected using the algorithm described previously (*7*) (http://genome.crg.es/CPE/).

Western blot. Samples from human brain were stored at –80°C and ground with a mortar in a frozen environment with liquid nitrogen to prevent thawing of the samples, resulting in tissue powder. For mouse, brains were quickly dissected on an ice-cold plate and the different structures stored at –80°C. Human and mouse extracts were prepared by homogenizing the brain areas in ice-cold extraction buffer (20 mM HEPES pH 7.4, 100 mM NaCl, 20 mM NaF, 1% Triton X-100, 1

mM sodium orthovanadate, 1 μM okadaic acid, 5 mM sodium pyrophosphate, 30 mM β-glycerophosphate, 5 mM EDTA and protease inhibitors (Complete, Roche, Cat. No 11697498001). Homogenates were centrifuged at 15000g for 15 min at 4°C. The resulting supernatant was collected, and protein content determined by Quick Start Bradford kit assay (Bio-Rad, 500-0203). Between 10 and 20 μg of total protein were electrophoresed on 10% SDS-polyacrylamide gels, transferred to a nitrocellulose blotting membrane (Amersham Protran 0.45 μm, GE Healthcare Life Sciences, 10600002) and blocked in TBS-T (150 mM NaCl, 20 mM Tris–HCl, pH 7.5, 0.1% Tween 20) supplemented with 5% non-fat dry milk. Membranes were incubated overnight at 4°C with the primary antibody in TBS-T supplemented with 5% non-fat dry milk, washed with TBS-T and next incubated with secondary HRP-conjugated anti-mouse IgG (1:2000, DAKO, P0447) or anti-rabbit IgG (1:2000, DAKO, P0448) and developed using the ECL detection kit (PerkinElmer, NEL105001EA). Images were scanned with a densitometer (Bio-Rad, GS-900) and quantified with Image Lab 5.2 (Bio-Rad).

Antibodies: Rabbit CPEB1 (1:350, Santacruz, sc-33193); rabbit CPEB2 (1:1000, Abcam, ab51069); rabbit CPEB3 (1:1000, Abcam, ab10883); rabbit CPEB4 (1:1000, Abcam, ab83009); rabbit AUTS2 (1:750, Sigma, HPA000390); rabbit KTN1 (1:1000, Proteintech, Cat. 19841-1-AP); rabbit ROCK1 (1:1000, Abcam, ab45171); rabbit SLC19A3 (1:1000, Sigma, HPA038898); rabbit SLC19A3 (1:1000, Proteintech, 13407-1-AP); mouse β-actin (1:25000, Sigma, A2228); rabbit vinculin (1:1000, Abcam, ab129002).

Poly(U) chromatography. Wild-type and R6/1 mice (n = 4) were sacrificed by cervical dislocation at the age of 7-8 months. Striatum was quickly dissected on an ice-cold plate and the pool of the four striata was immersed in ice-cold RNAlater (Sigma, R0901). Striatum pool was homogenized

and total RNA was extracted and purified with Ultraspec (Biotecx, BL-10050), frozen and stored at -80°C until use.

The poly(A) RNA fraction was purified by poly(U) chromatography. Poly(U)-agarose (Sigma, p8563) was suspended in swelling buffer (0.05 M Tris-HCl, pH 7.5, 1 M NaCl) 35 ml/g, incubated overnight at room temperature and loaded into the chromatography column. An aliquot of total RNA was stored at –80°C ("Input") and the rest was incubated with sample buffer (0.01 M Tris-HCl, pH 7.5, 1 mM EDTA, 1% SDS) for 5 min at 65°C and chilled on ice. Binding buffer was added (0.05 M Tris-HCl, pH 7.5, 0.7 M NaCl, 10 mM EDTA, 25% [v/v] formamide) and then the sample was loaded into the poly(U)-agarose chromatography column (Mobitec, M1002s) and incubated for 30 min at room temperature (25°C) with agitation. Next, the column containing the sample was washed three times at 25°C and six times at 55°C with washing buffer (0.05 M Tris-HCl, pH 7.5, 0.1 M NaCl, 10 mM EDTA, 25% [v/v] formamide). The 55°C washes were collected and stored at –80°C ("short poly(A)-tail fraction"). The remaining poly(A) RNA ("long poly(A)-tail fraction") was eluted with elution buffer (0.05 M HEPES, pH 7, 10 mM EDTA, 90% [v/v] formamide) at 55°C and stored at –80°C. The RNA of the two poly(A) fractions was precipitated by adding 1 volume of isopropanol, 1/10th volumes of sodium acetate 3M pH 5.2 and 20 µg of glycogen (Sigma, G1767). Samples were incubated at –20°C for 20 min and centrifuged 15 min at 14000g at 4°C. Supernatant was removed, and the pellet was washed with 750 µL of ethanol and centrifuged at 14000g and 4°C for 5 min. The supernatant was removed and the pellet was air-dried for 5 min. After RNA was resuspended in 300 µL of nuclease-free water, 300 µL of acid phenol:chloroform (5:1) was added. Samples were vortexed and centrifuged for 10 min at 14000 g at 4°C.

RNA was quantified with the Qubit Fluorimeter using the Qubit RNA Hs Assay kit (Thermo-Fisher Scientific, Q32852). RNA integrity QC was performed with Agilent Bioanalyzer 2100, using RNA Nano Assay (Agilent Technologies 5067-1511) and RNA Pico Assay (Agilent Technologies 5067-1513).

cDNA library preparation and amplification were performed according to the manufacturer's instructions (Sigma-Aldrich) for WTA2 kit using as a template from 2 to 5 ng of Total RNA. cDNA was amplified for 22 cycles and purified using PureLink Quick PCR Purification Kit (Invitrogen, K310001). Amplified cDNA was quantified using a Nanodrop ND-1000 (Thermo- Fisher Scientific), and 8 µg of cDNA from each sample was fragmented and labelled with GeneChip Mapping 250K Nsp assay kit (Affymetrix, 900753) following the manufacturer's instructions.

Hybridization was performed using the GeneAtlas Hyb, Wash and Stain Kit for 3' IVT arrays. Samples ready to hybridize were denatured at 96°C for 10 min prior to incubation into Mouse MG-430 PM Array Strip (Affymetrix, 901570), the hybridization was performed for 16 h at 45°C in the GeneAtlas Hybridization Oven (Affymetrix, 00-0331). Washing and stain steps after hybridization were performed in the GeneAtlas Fluidics Station (Affymetrix, 00-0079), following the specific script for Mouse MG-430 PM Arrays. Finally, arrays were scanned with GeneAtlas Scanner (Affymetrix) using default parameters, and CEL files for bioinformatics analysis were generated with the GeneAtlas software (Affymetrix).

Microarray samples were processed using R (R Development Core Team, 2014) and Bioconductor (*40*). Raw CEL files were normalized using RMA background correction and summarization (*41*). Standard quality controls were performed in order to identify abnormal samples (*42*) regarding: a) spatial artifacts in the hybridization process (scan images and pseudo-

images from probe level models); b) intensity dependences of differences between chips (MvA plots); c) RNA quality (RNA digest plot); and d) global intensity levels (boxplot of perfect match log-intensity distributions before and after normalization and RLE plots). Probeset annotation was performed using the information available in Affymetrix web page (https://www.affymetrix.com/analysis/index.affx) using version na35.

Expression values were adjusted for technical biases as described in (*43*), using a linear model and implemented with the R package "limma" (*44*). For each biological replicate the log2 fold change was computed between "WASH" and "ELUTED" samples and used to find significant differences between WT vs R6/1 mice. Differential expression was performed using a linear model with fluidics and amplification batch as covariates. Fold-change value of < -1.5 in at least one probe indicated that the transcript is shortened in R6/1 mice; ≥ 1.5, that it is lengthened; and the values in between mean no change. If the same transcript showed opposite results for different probes, it was considered as not changed.

Real-time quantitative reverse transcriptase-PCR. Quantification was performed by real-time PCR using a CFX 384 Real Time System C1000 Thermal Cycler (Bio-Rad) in combination with SsoFast Eva Green (Bio-Rad, CN 172-5204) and 0.25 μM of primer pair was used. Data were analysed by GenEx 5.3.7 software (Multid AnaLyses AB). The mRNA levels were normalized first relative to total RNA and then relative to the 18S ribosome subunit, β-ACTIN, GAPDH and β-TUBULIN gene expression in each sample.

Human primers

CPEB1	**Forward**	5'-ggcagccatcttgaacga-3'
	Reverse	5'-aagtcacacgaccagaacca-3'
CPEB2	**Forward**	5'-gcctcataaagcagaaagcaa-3'
	Reverse	5'-agcatcaatgagtgcctgaa-3'
	Forward	5'-gaacgctactctagaaaggtgtttg-3'

CPEB3	**Reverse**	5'-cgaaagctggcagtgatct-3'
CPEB4	**Forward**	5'-cactgtttccaatggaagatgg-3'
	Reverse	5'-ggtgaacccaggccactatg-3'
AUTS2	**Forward**	5'-gaagcggagagagtccacct-3'
	Reverse	5'-tcctgaggcttaagtgctacatc-3'
ROCK1	**Forward**	5'-tcccctcgaacgctttctac-3'
	Reverse	5'-tgtatttttgaccactttccgga-3'
KTN1	**Forward**	5'-atttcagaaagagagaaagaaataagtgg-3'
	Reverse	5'-tgttcaactgcatccttcaaaga-3'
SLC19A3	**Forward**	5'-agttcctggatttaccccactg-3'
	Reverse	5'-ggttctgagggtctcatcatgg-3'
18S	**Forward**	5'-atccattggagggcaagtc-3'
	Reverse	5'-gctcccaagatccaactacg-3'
β-TUBULIN	**Forward**	5'-ctttgtggaatggatcccca-3'
	Reverse	5'-gactgccatcttgaggcca-3'

GAPDH and β-ACTIN (Tataa biocenter, qA-01-0101S, qA-01-0104S)

Mouse primers

Cpeb1	**Forward**	5'-ttatctgcagctcacaacctg-3'
	Reverse	5'-gcaaaagtacttgaagcagacct-3'
Cpeb2	**Forward**	5'-ctgcagcagaggaactcgta-3'
	Reverse	5'-ggttgctccaaggagactgt-3'
Cpeb3	**Forward**	5'-aaaacccagccccagtct-3'
	Reverse	5'-gcttggggatctctgagga-3'
Cpeb4	**Forward**	5'-caaatcttattttccaccaaaagg-3'
	Reverse	5'-catcaatgagagcctgaacaga-3'
Auts2	**Forward**	5'-cctccaggccctagtctctt-3'
	Reverse	5'-aaggggtcccagtaggatgt-3'
Rock1	**Forward**	5'-gatcccaaatcggaagtgaa-3'
	Reverse	5'-tcataaaccagggcatcca-3'
Ktn1	**Forward**	5'-ttaaaagctgaagtgcagaaattg-3'
	Reverse	5'-acctcatgtgcggtagcag-3'
Slc19a3	**Forward**	5'-gagcagtagaggccatagcaa-3'
	Reverse	5'-ccttcagatagcccactgaga-3'
18s	**Forward**	5'-ctcaacacgggaaacctcac-3'
	Reverse	5'-cgctccaccaactaagaacg-3'

Gapdh	**Forward**	5'-ctcccactcttccaccttcg-3'
	Reverse	5'-cataccaggaaatgagcttgacaa-3'
β-Actin	**Forward**	5'-ctaaggccaaccgtgaaaag-3'
	Reverse	5'-accagaggcatacagggaca-3'
β-Tubulin	**Forward**	5'-gacctatcatggggacagtga-3'
	Reverse	5'-cggctctgggaacatagttt-3'

Immunohistochemical analyses. Sample preparation. For human samples, formalin-fixed (4%, 24 h), paraffin-embedded, 5 μm thick sections mounted on superfrost-plus tissue slides (Menzel-Gläser, 631-9483) were deparaffinized. For mouse samples, left hemispheres were fixed overnight in 4% paraformaldehyde, cryopreserved for 72h in 30% sucrose in PBS, included in optimum cutting temperature (OCT) compound (Tissue-Tek, Sakura Finetek Europe, ref. 4583), frozen and stored at −80 °C until use. 30 μm sagittal sections were cut on a cryostat (Thermo Scientific), collected and stored free floating in glycol containing buffer (30% glycerol, 30% ethylene glycol in 0.02 M phosphate buffer) at −20 °C.

Immunohistochemistry. For human sections, peroxidase activity was quenched with 0.3% H_2O_2 in methanol for 30 min, followed by antigen retrieval with 10 mM pH 6.0 citrate buffer heated by microwave for 15 min. Mouse sections were washed in PBS, immersed in 0.3% H2O2 in PBS for 45 min to quench endogenous peroxidase activity and blocked for 1 h in blocking solution (PBS containing 0.5% Fetal Bovine Serum, 0.3% Triton X-100 and 1% BSA). Human and mice sections were incubated overnight at 4°C with the corresponding primary antibody diluted in blocking solution. After washing, sections were incubated first with biotinylated anti-rabbit or anti-mouse secondary antibody and then with avidin-biotin complex using the Elite Vectastain kit (Vector Laboratories, PK-6101 and PK-6102). Chromogen reactions were performed with diaminobenzidine (SIGMAFAST DAB, Sigma, D4293) for 10 min. Mouse sections were mounted on glass slides and coverslipped with Mowiol (Calbiochem, Cat. 475904) while human slides were

dehydrated and coverslipped with DePeX (Serva). Images were captured using an Axioskop2 plus (Zeiss) microscope with an DMC6200 camera (Leica).

Antibodies: Rabbit SLC19A3 (1:1000, Sigma, HPA038898), Rabbit Cleaved Caspase-3 (1:100, Cell Signaling, 9661), Rabbit DARPP32 (1:3000, BD, 611520), Rabbit CPEB4 (1:1000, Sigma, HPA038394).

Immunofluorescence. Mouse sections were selected, washed in PBS and pretreated with 0.1% Triton X-100 for 30 min, 1 M glycine for 15 min and blocking solution (1% BSA, 0.3% FBS and 0.1% Triton X-100) for 1 h. Sections were then incubated overnight at 4 °C with mouse anti-CPEB4 (1:1500, home-made) and goat anti-huntingtin (1:200, N-18 Santa Cruz, sc-8767) in blocking solution. After washing in PBS, sections were incubated with anti-goat Alexa 555 (1:500, ThermoFisher, A-21432) and anti-mouse Alexa 488 (1:500, ThermoFisher, A-21202) for 1 h. Finally, sections were mounted on glass slides, coverslipped with Mowiol (Calbiochem, 475904) and maintained at 4 °C.

Quantification of cleaved caspase-3 positive cells. Animals were analysed at the age of 19 weeks. The total number of immunopositive cells in three sagittal sections (lateral coordinates 0.72, 1.92 and 3.00 mm) was quantified per each animal using an Olympus BX41 microscope with an Olympus camera DP-70 (Olympus Denmark A/S). Means per genotype or +/- treatment were used for statistical comparison.

Striatal area quantification. Animals were analysed at the age of 19 weeks. The striatal area was measured by Darpp32 positive immunostaining in sagittal sections (lateral coordinate 2.64) using an Olympus BX41 microscope with an Olympus camera DP-70 (Olympus Denmark A/S). Means per genotype or +/- treatment were used for statistical comparison.

Mouse brain vessels extraction. Brain microvessels were isolated by a modification of methods described previously (*45, 46*). Wild-type and R6/1 mice (n=5) were killed by cervical dislocation and brains were extracted from the skull. The meninges were carefully removed and gray matter was minced and homogenized in 5 volumes of Buffer A (mM): 103 NaCl, 4.7 KCl, 1.2 KH2PO4, 1.2 MgSO4, 15 HEPES, pH 7.4, 10 Glucose and 25 NaHCO3 with a Teflon-glass homogenizer. Homogenization was achieved with 6 to 10 upward and downward strokes. The homogenates were centrifuged at 3500g for 10 min at 4°C. The pellets were resuspended in 15% dextran (MW = 79,500). Samples were then centrifuged again for 15 min at 5000g at 4°C. The pellets were resuspended in 50 ml of Buffer A and passed over a 180-µm-pore-size nylon net (Merck, NY8H04700). Once the vessels were isolated, they were resuspended in extraction buffer (see Western blot) and 5x loading buffer (Tris 0.5M pH 6.8, SDS 10%, Glycerol 85%, 2% β-mercaptoethanol, 0.01% bromophenol blue) and then sonicated in a sonicator (Sartoirus, Labsonic M) for 10s, 100% amplitude, cycle 1.

Thiamine determination. CSF, total blood and striatum samples were collected from mice or human. Samples were collected in a light-protected vial and stored at -80°C. Cortex and striatum samples were homogenized and protein content determined by Quick Start Bradford kit assay (Bio-Rad, 500-0203). The concentration of free thiamine and its derivatives (TPP and TMP) were analysed by a commercially available kit for Vitamin B1 determination (Chromsystems, Munich, Germany), using a high-performance liquid chromatography (HPLC) method for its separation and quantification, according to a modified reported procedure (*47*). Samples were put in an autosampler protected from light, and 50 µl were applied with a flow rate of 1.0 ml/min to an HPLC system (Agilent Technologies, 1200 Series) equipped with a reversed phase analytical column (Agilent, Eclipse Plus C18, 3.5µm, 4.6x150mm) with fluorescence detection (Ex

wavelength=375nm; Em wavelength=435nm). Briefly, the mobile phase consisted of linear gradient of sodium phosphate buffer (pH 7.0) and methanol. Chromatographic data were processed with LC ChemStation software (Agilent Technologies). Finally, the concentration of thiamine derivatives was calculated in brain tissue in nmol/g protein and in total blood and CSF in nmol/L.

Magnetic resonance imaging. Mice were placed into the centre of the volume RF (radiofrequency) coil and positioned in the magnet under continuous inhalation anaesthesia via a nose cone. A respiratory sensor connected to a monitoring system (SA Instruments, Stony Brook, NY) was placed under the abdomen to monitor the rate and depth of respiration. Mice were anesthetized with a 2% isoflurane in 1L of oxygen in an induction chamber and the flow of anaesthetic gas was constantly regulated to maintain a breathing rate of 50 +/- 20 bpm. Animal temperature was maintained at approximately at 37°C by passing warm water through a heat exchanger machine into the animal platform. The physiological state of the animals was monitored using a Magnetic Resonance Imaging (MRI) compatible small animal gating system by SA Instruments (Stony Brook, NY; http://www.i4sa.com/) that controlled the respiratory rate.

The MRI experiments were performed on a Bruker Pharmascan system (Bruker Medical Gmbh, Ettlingen, Germany) using a 7.0-T horizontal-bore superconducting magnet, equipped with a 1H selective birdcage resonator of 23 mm and a Bruker gradient insert with 90 mm of diameter (maximum intensity 36 G/cm) by the MRI facility at the Instituto de Investigaciones Biomédicas "Alberto Sols" (Madrid, Spain). All data were acquired using a Hewlett-Packard console running Paravision 5.1 software (Bruker Medical Gmbh) operating on a Linux platform.

T2-weighted (T2-W) spin-echo images were acquired with a rapid acquisition with relaxation enhancement (RARE) sequence in axial orientations and the following parameters: TR = 3000 ms, TE = 14,7ms, RARE factor = 8, Av = 6, FOV = 2.3cm, acquisition matrix = 256 ×

256, slice thickness = 1.00 mm without gap and number of slices = 16. To calculate the striatum volume in mm3, area was measured in all series of images obtained in MRI-T2W for each animal using ImageJ software (Wayne Rasband, NIH, Bethesda, MD, USA).

1H MR spectroscopy study was performed in the striatum region. The *in vivo* spectroscopy protocol used a Point-Resolved Spatially Spectroscopy (PRESS), combined with VAPOR water suppression and employed the following parameters: TR = 3000 ms, TE = 35 ms, Av = 128, voxel volume = 3 mm3. Before acquisition the automatic shimming procedure FASTMAP (*48*) was used to achieve optimal uniformity of the magnetic field across the voxel volume. All 1H spectra were automatically analysed using LC Model version 6.2 OR (Stephen Provencher, Oakville, ON; Canada). Means per genotype or +/- treatment were used for statistical comparison.

Behavioral testing. *Rotarod test*: Motor coordination was measured in an accelerating rotarod apparatus (Ugo Basile). Mice were pre-trained during two days at a constant speed, the first day: 4 trials of 1 min at 4rpm and the second day: 4 trials of 1 min at 8rpm. On the third day, rotarod was set to accelerate from 4 to 40 rpm over 5 min and mice were tested four times. During accelerating trials, the latency to fall from the rod was measured.

Inverted grid test: Muscular strength was examined placing the mice in the center of a wire grid that is rotated to an inverted position over 10 s and held steadily 50cm above a padded surface. Latency to fall from the grid was measured (maximum: 300 s, two trials).

Open field test: Locomotor activity was measured in clear Plexiglas® boxes measuring 27.5cm x 27.5cm, outfitted with photo-beam detectors for monitoring horizontal and vertical activity. Activity levels were recorded with a MED Associates' Activity Monitor (MED Associates, St. Albans, VT) and were analyzed with the MED Associates' Activity Monitor Data Analysis v.5.93.773 software. Mice were placed in the center of the open-field apparatus and left to move

freely. Data were individually recorded for each animal during 15 min. Ambulatory distance walked was measured.

Data analysis. Statistical analysis was performed with SPSS 26.0 (SPSS® Statistic IBM®). Data are represented as Mean ± s.e.m (Standard Error of the Mean) with 95% confidence interval. In box plots, box segments show median, 25th and 75th percentiles, whiskers above and below show the locations of the minimum and maximum. Higher or lower points (outliers) were plotted individually or not plotted. The normality of the data was analyzed by Shapiro-Wilk test ($n < 50$) or o Kolmogorov-Smirnov ($n > 50$). Homogeneity of variance was analyzed by Levene test. For comparison of two independent groups two-tail unpaired t-Student's test (data with normal distribution), Mann-Whitney-Wilcoxon or Kolmogorov-Smirnov tests (with non-normal distribution) was performed. To compare dependent measurements, we used a paired t-test (normal distribution) or Wilcoxon signed-rank tests (non-normal). For multiple comparisons, data with a normal distribution were analyzed by one way-ANOVA test followed by a Tukey's or a Games-Howell's post-hoc test. Statistical significance of non-parametric data for multiple comparisons was determined by Kruskal-Wallis One-way ANOVA test. Enrichment tests were carried out by using one-sided Fisher's exact test. A critical value for significance of $P < 0.05$ was used throughout the study.

List of Supplementary Materials

Figure S1. CPEB status in HD and HD mice.

Figure S2. ThTr2 in HD mice.

Table S1. PolyU chromatography/Gene chip analysis + Gene ontology analysis

References

1. F. O. Walker, Huntington's disease. *Lancet (London, England)* **369**, 218-228 (2007).
2. S. J. Tabrizi, R. Ghosh, B. R. Leavitt, Huntingtin Lowering Strategies for Disease Modification in Huntington's Disease. *Neuron* **101**, 801-819 (2019).
3. R. A. Barker, M. Fujimaki, P. Rogers, D. C. Rubinsztein, Huntingtin-lowering strategies for Huntington's disease. *Expert Opin Investig Drugs*, (2020).
4. H. T. Orr, H. Y. Zoghbi, Trinucleotide repeat disorders. *Annual review of neuroscience* **30**, 575-621 (2007).
5. L. B. Li, Z. Yu, X. Teng, N. M. Bonini, RNA toxicity is a component of ataxin-3 degeneration in Drosophila. *Nature* **453**, 1107-1111 (2008).
6. S. Y. Shieh, N. M. Bonini, Genes and pathways affected by CAG-repeat RNA-based toxicity in Drosophila. *Human molecular genetics* **20**, 4810-4821 (2011).
7. M. Pique, J. M. Lopez, S. Foissac, R. Guigo, R. Mendez, A combinatorial code for CPE-mediated translational control. *Cell* **132**, 434-448 (2008).
8. A. Parras *et al.*, Autism-like phenotype and risk gene mRNA deadenylation by CPEB4 mis-splicing. *Nature* **560**, 441-446 (2018).
9. M. Ivshina, P. Lasko, J. D. Richter, Cytoplasmic polyadenylation element binding proteins in development, health, and disease. *Annual review of cell and developmental biology* **30**, 393-415 (2014).
10. L. Weill, E. Belloc, F. A. Bava, R. Mendez, Translational control by changes in poly(A) tail length: recycling mRNAs. *Nature structural & molecular biology* **19**, 577-585 (2012).
11. K. Si, Y. B. Choi, E. White-Grindley, A. Majumdar, E. R. Kandel, Aplysia CPEB can form prion-like multimers in sensory neurons that contribute to long-term facilitation. *Cell* **140**, 421-435 (2010).
12. E. Ortiz-Zapater *et al.*, Key contribution of CPEB4-mediated translational control to cancer progression. *Nature medicine* **18**, 83-90 (2011).
13. E. Perez-Guijarro *et al.*, Lineage-specific roles of the cytoplasmic polyadenylation factor CPEB4 in the regulation of melanoma drivers. *Nature communications* **7**, 13418 (2016).
14. V. Calderone *et al.*, Sequential Functions of CPEB1 and CPEB4 Regulate Pathologic Expression of Vascular Endothelial Growth Factor and Angiogenesis in Chronic Liver Disease. *Gastroenterology* **150**, 982-997 e930 (2016).
15. A. Parras *et al.*, Polyadenylation of mRNA as a novel regulatory mechanism of gene expression in temporal lobe epilepsy. *Brain* **143**, 2139-2153 (2020).
16. I. M. Alexandrov *et al.*, Cytoplasmic polyadenylation element binding protein deficiency stimulates PTEN and Stat3 mRNA translation and induces hepatic insulin resistance. *PLoS genetics* **8**, e1002457 (2012).
17. K. Si, S. Lindquist, E. R. Kandel, A neuronal isoform of the aplysia CPEB has prion-like properties. *Cell* **115**, 879-891 (2003).
18. M. Fernandez-Nogales *et al.*, Huntington's disease is a four-repeat tauopathy with tau nuclear rods. *Nature medicine* **20**, 881-885 (2014).
19. M. Fernandez-Nogales *et al.*, Decreased glycogen synthase kinase-3 levels and activity contribute to Huntington's disease. *Human molecular genetics* **24**, 5040-5052 (2015).
20. G. Huez *et al.*, Degradation of deadenylated rabbit alpha-globin mRNA in Xenopus oocytes is associated with its translation. *Nature* **266**, 473-474 (1977).
21. D. P. Hibar *et al.*, Common genetic variants influence human subcortical brain structures. *Nature* **520**, 224-229 (2015).
22. W. Q. Zeng *et al.*, Biotin-responsive basal ganglia disease maps to 2q36.3 and is due to mutations in SLC19A3. *American journal of human genetics* **77**, 16-26 (2005).
23. J. D. Ortigoza-Escobar *et al.*, Thiamine deficiency in childhood with attention to genetic causes: Survival and outcome predictors. *Annals of neurology* **82**, 317-330 (2017).
24. A. Rajgopal, A. Edmondnson, I. D. Goldman, R. Zhao, SLC19A3 encodes a second thiamine transporter ThTr2. *Biochimica et biophysica acta* **1537**, 175-178 (2001).
25. J. D. Ortigoza-Escobar *et al.*, Free-thiamine is a potential biomarker of thiamine transporter-2 deficiency: a treatable cause of Leigh syndrome. *Brain* **139**, 31-38 (2016).
26. A. Marce-Grau, L. Marti-Sanchez, H. Baide-Mairena, J. D. Ortigoza-Escobar, B. Perez-Duenas, Genetic defects of thiamine transport and metabolism: A review of clinical phenotypes, genetics, and functional studies. *J Inherit Metab Dis* **42**, 581-597 (2019).
27. J. D. Ortigoza-Escobar *et al.*, Treatment of genetic defects of thiamine transport and metabolism. *Expert Rev Neurother* **16**, 755-763 (2016).

28. T. I. Vlasova, S. L. Stratton, A. M. Wells, N. I. Mock, D. M. Mock, Biotin deficiency reduces expression of SLC19A3, a potential biotin transporter, in leukocytes from human blood. *J Nutr* **135**, 42-47 (2005).
29. T. B. Haack *et al.*, Infantile Leigh-like syndrome caused by SLC19A3 mutations is a treatable disease. *Brain* **137**, e295 (2014).
30. L. Bettendorff, M. Peeters, P. Wins, E. Schoffeniels, Metabolism of thiamine triphosphate in rat brain: correlation with chloride permeability. *Journal of neurochemistry* **60**, 423-434 (1993).
31. P. T. Ozand *et al.*, Biotin-responsive basal ganglia disease: a novel entity. *Brain* **121 (Pt 7)**, 1267-1279 (1998).
32. T. Heikkinen *et al.*, Characterization of neurophysiological and behavioral changes, MRI brain volumetry and 1H MRS in zQ175 knock-in mouse model of Huntington's disease. *PloS one* **7**, e50717 (2012).
33. A. Yamamoto, J. J. Lucas, R. Hen, Reversal of neuropathology and motor dysfunction in a conditional model of Huntington's disease. *Cell* **101**, 57-66. (2000).
34. H. B. Kordasiewicz *et al.*, Sustained therapeutic reversal of Huntington's disease by transient repression of huntingtin synthesis. *Neuron* **74**, 1031-1044 (2012).
35. M. Diaz-Hernandez *et al.*, Full motor recovery despite striatal neuron loss and formation of irreversible amyloid-like inclusions in a conditional mouse model of Huntington's disease. *J Neurosci* **25**, 9773-9781 (2005).
36. C. Estevez-Fraga, M. D. Flower, S. J. Tabrizi, Therapeutic strategies for Huntington's disease. *Current opinion in neurology* **33**, 508-518 (2020).
37. S. J. Tabrizi, M. D. Flower, C. A. Ross, E. J. Wild, Huntington disease: new insights into molecular pathogenesis and therapeutic opportunities. *Nat Rev Neurol*, (2020).
38. L. Mangiarini *et al.*, Exon 1 of the HD gene with an expanded CAG repeat is sufficient to cause a progressive neurological phenotype in transgenic mice. *Cell* **87**, 493-506 (1996).
39. W. Huang da, B. T. Sherman, R. A. Lempicki, Systematic and integrative analysis of large gene lists using DAVID bioinformatics resources. *Nat Protoc* **4**, 44-57 (2009).
40. R. C. Gentleman *et al.*, Bioconductor: open software development for computational biology and bioinformatics. *Genome Biol* **5**, R80 (2004).
41. R. A. Irizarry *et al.*, Exploration, normalization, and summaries of high density oligonucleotide array probe level data. *Biostatistics* **4**, 249-264 (2003).
42. R. Gentleman, V. J. Carey, S. Dudoit, W. Huber, R. A. Irizarry, *Bioinformatics and Computational Biology Solutions Using R and Bioconductor*. (Springer Science+Business Media, Inc. %@ 978-0-387-29362-2, New York, NY, 2005).
43. A. C. Eklund, Z. Szallasi, Correction of technical bias in clinical microarray data improves concordance with known biological information. *Genome Biol* **9**, R26 (2008).
44. M. E. Ritchie *et al.*, limma powers differential expression analyses for RNA-sequencing and microarray studies. *Nucleic acids research* **43**, e47 (2015).
45. R. E. Catalan, A. M. Martinez, M. D. Aragones, F. Hernandez, Identification of nitric oxide synthases in isolated bovine brain vessels. *Neurosci Res* **25**, 195-199 (1996).
46. J. E. Hardebo, P. C. Emson, B. Falck, C. Owman, E. Rosengren, Enzymes related to monoamine transmitter metabolism in brain microvessels. *Journal of neurochemistry* **35**, 1388-1393 (1980).
47. J. A. Mayr *et al.*, Lipoic acid synthetase deficiency causes neonatal-onset epilepsy, defective mitochondrial energy metabolism, and glycine elevation. *American journal of human genetics* **89**, 792-797 (2011).
48. R. Gruetter, Automatic, localized in vivo adjustment of all first- and second-order shim coils. *Magn Reson Med* **29**, 804-811 (1993).

Acknowledgments: We thank Celia Pérez-Cerdá for advice on thiamine determination techniques, Miriam Lucas for excellent technical assistance and the following core facilities: CBMSO-Genomics & Massive Sequencing, IRB-Functional Genomic and IRB-Bioinformatics and Biostatistics, IIBM-High Field Magnetic Resonance Imaging and Spectroscopy. **Funding**: This work was supported by CiberNed-ISCIII collaborative grants 2013/09-2 to J.J.L, 2015-2/06 and 2018/06-5 to J.J.L and T.I., and by grants SAF2015-65371-R (MINECO/AEI/FEDER, UE) and by grants from Spanish Ministry of Science, Innovation and Universities (MINECO/MICINN): RTI2018-096322-B-I00 (MCIU/AEI/FEDER, UE) to J.J.L., SAF2017-88885-R (MINECO/AEI/FEDER, UE) to T.I., BFU2014-54122-P (MINECO/AEI/FEDER, UE) to R.M., and ISCIII-FEDER (PI17/00199) to P.N., by the European Union FEDER funds, the Fundación Botín by the Banco Santander through its Santander Universities Global Division, by Fundación BBVA and by Fundación Ramón Areces. A.P. and S.P. were recipients of FPI fellowships from MICINN/MINECO, A.P. was also recipient of a contract from CIBERNED, J.P.U. was contracted by SAF2017-88885-R (MINECO/AEI/FEDER, UE), D.M-G. was supported by the "Río Hortega" programme [CM18/00142] from ISCIII-FEDER, A.E. was recipient of Juan de la Cierva contracts from MICINN/MINECO.

Author contributions: S.P., A.P. and M.S-G. contributed to study design and were involved in all assays, data collection and analysis. J.P-U. performed analysis of RMN and spectroscopy. M.C, M.D.V and L. M-S. contributed with HPLC analysis. E.F., A.E, P.G-E. and N.W performed Western blotting. I.H.H performed bioinformatics analysis. H.A. and E.B. contributed to RIP and PolyU chromatography experiments. D.M-G., P.M, I.F and J.L.L-S. contributed collecting human samples. F.H., J.J.G., R.A. and B.P. made intellectual contributions to experimental design and discussion. P.N., T.I., X.W.Y., R.M and J.J.L supervised the study and designed experiments.

J.J.L. wrote the paper with input from all authors. **Competing Interests statement:** The authors declare no competing Interests. **Data and materials availability:** Tissue, biological specimens or data used in this research were obtained from Institute of Neuropathology Brain Bank (HUBICO-IDIBELL, Hospitalet de Llobregat, Spain), the Neurological Tissue Bank of the IDIBAPS Biobank (Barcelona, Spain), the Banco de Tejidos Fundación Cien (BT-CIEN, Madrid, Spain), Hospital Universitario Ramón y Cajal (Madrid, Spain), HUVR-IBiS Biobank (Andalusian Public Health System Biobank and ISCIII-Red de Biobancos PT13/0010/0056) and the Netherlands Brain Bank (Amsterdam, The Netherlands). We thank the HD patients and families who participated in the tissue donation programs.

Figures Legends:

Fig. 1. **CPEB1/4 imbalance in HD striatum**. (**A,B**) CPEB1 and CPEB4 protein levels in (**A**) control or HD striatum, and (**B**) wild-type or R6/1 mice striatum. (**C**) CPEB4 immunohistochemistry in wild-type or R6/1 mice striatum. (**D**) CPEB4 (green) and HTT (red) immunofluorescence in wild-type or R6/1 mice striatum. (A,B) Two-sided unpaired t-test. Graphs show mean ± s.e.m.

Fig. 2. **Attenuation of R6/1 phenotype through CPEB4 overexpression**. (**A, D**) Latency to fall off the rotarod for (**A**) wild-type, CPEB1$^{+/-}$, R6/1 or R6/1:CPEB1$^{+/-}$ mice and (**D**) wild-type, TgCPEB4, R6/1 or R6/1:TgCPEB4 mice. (**B, E**) Ambulatory distance travelled for (**B**) wild-type, CPEB1$^{+/-}$, R6/1 or R6/1:CPEB1$^{+/-}$ mice (22 weeks-old) and (**E**) wild-type, TgCPEB4, R6/1 or R6/1:TgCPEB4 mice (18 weeks-old respect to 10 weeks-old). (**C, F**) Latency to fall off the inverted grid test for (**C**) wild-type, CPEB1$^{+/-}$, R6/1 or R6/1:CPEB1$^{+/-}$ mice (22 weeks-old) and (**F**) wild-type, TgCPEB4, R6/1 or R6/1:TgCPEB4 mice (22 weeks-old). One way-ANOVA followed by Tukey's post-hoc test. Graphs show mean ± s.e.m.

Fig. 3. **Global poly(A) alteration in HD affects neurodegeneration related genes**. (**A**) Poly(U) chromatography design and percentage of transcripts with lengthened or shortened poly(A) in R6/1 striatum (FC ≤ -1.5 & ≥ 1.5). (**B**) Gene counts from GO analysis of mRNAs with altered poly(A)-tail (FC ≤ -2 & ≥ 2). (**C**) Venn diagram of neurodegenerative disease-related genes with altered poly(A) (FC ≤ -1.5 & ≥ 1.5); Mendelian disease–linked genes are shown in bold. (B) Benjamini–Hochberg corrected P-value.

Fig. 4. **Top deadenylated transcripts show decreased protein levels**. (**A**) Incidence of CPEs in 3'UTR according to the mRNA poly(A) change. (**B**) Symbol, gene name and number of CPEs of most deadenylated transcripts in R6/1 mice. (**C**) AUTS2, ROCK1 and KTN1 protein and mRNA levels in control or HD striatum, and wild-type or R6/1 mouse striatum. (A) One-sided Fisher's exact-test. (C) Two-tailed unpaired t-test. Graphs show mean ± s.e.m.

Fig. 5. **Decreased ThTr2 and thiamine in HD**. (**A, B**) SLC19A3 protein (ThTr2) and mRNA levels (**A**) and ThTr2 immunohistochemistry (**B**) in control and HD striatum and cortex. (**C**) Quantification of thiamines in control and HD CSF (nmol/L) and whole-blood (nmol/L). (**D**) Quantification of thiamines in control and HD striatum (nmol/g protein). Two-tailed unpaired t-test. Graphs show mean ± s.e.m.

Fig. 6. **Attenuation of HD mice phenotype upon biotin+thiamine (B+T)**. (**A, B**) Concentration of thiamines in striatum (nmol/g protein) of (**A**) wild-type or zQ175 mice with or without B+T and (**B**) wild-type or R6/1 mice with or without B+T. (**C, D**) In vivo T2-weighted MRI quantification of striatal volume of (**C**) untreated 17 week-old wild type or zQ175 mice and (**D**) treated and untreated 24 week-old wild type or zQ175 mice. (**E**) Phosphocreatine concentration (left) by MR spectroscopy in striatum of wild-type or zQ175 mice with or without B+T (example of spectra on the right). (**F**) Latency to fall off the rotarod for wild-type or R6/1 mice with or without B+T. (**G**) Latency to fall off the inverted grid test for wild-type or R6/1 mice with or without B+T. (**H**) DARPP32-

immunostained striatal area in wild-type or R6/1 mice with or without B+T. (**I**) Quantification of Cleaved-caspase3 positive cells in brain of wild-type or R6/1 mice with or without B+T. (C) Two-tailed unpaired t-test; (A,B,D,E,F,G,H,I) One way-ANOVA followed by Tukey's post-hoc test. Graphs show mean ± s.e.m.

Figure S1. **CPEB status in HD and HD mice**. (**A, B**) CPEB2 and CPEB3 protein levels in (**A**) control or HD striatum, and (**B**) wild-type or R6/1 mice striatum. (**C**) CPEB1 and CPEB4 protein levels in wild-type or zQ175 mice striatum. (**D, E**) CPEB1 and CPEB4 mRNA levels in (**D**) control or HD striatum, and (**E**) wild-type or R6/1 mice striatum. Two-tailed unpaired t-test. Graphs show mean ± s.e.m.

Figure S2. **ThTr2 in HD mice**. (**A, B**) SLC19A3 protein (ThTr2) levels in (**A**) wild-type or R6/1 mouse and in (**B**) wild-type or zQ175 brain vessels.

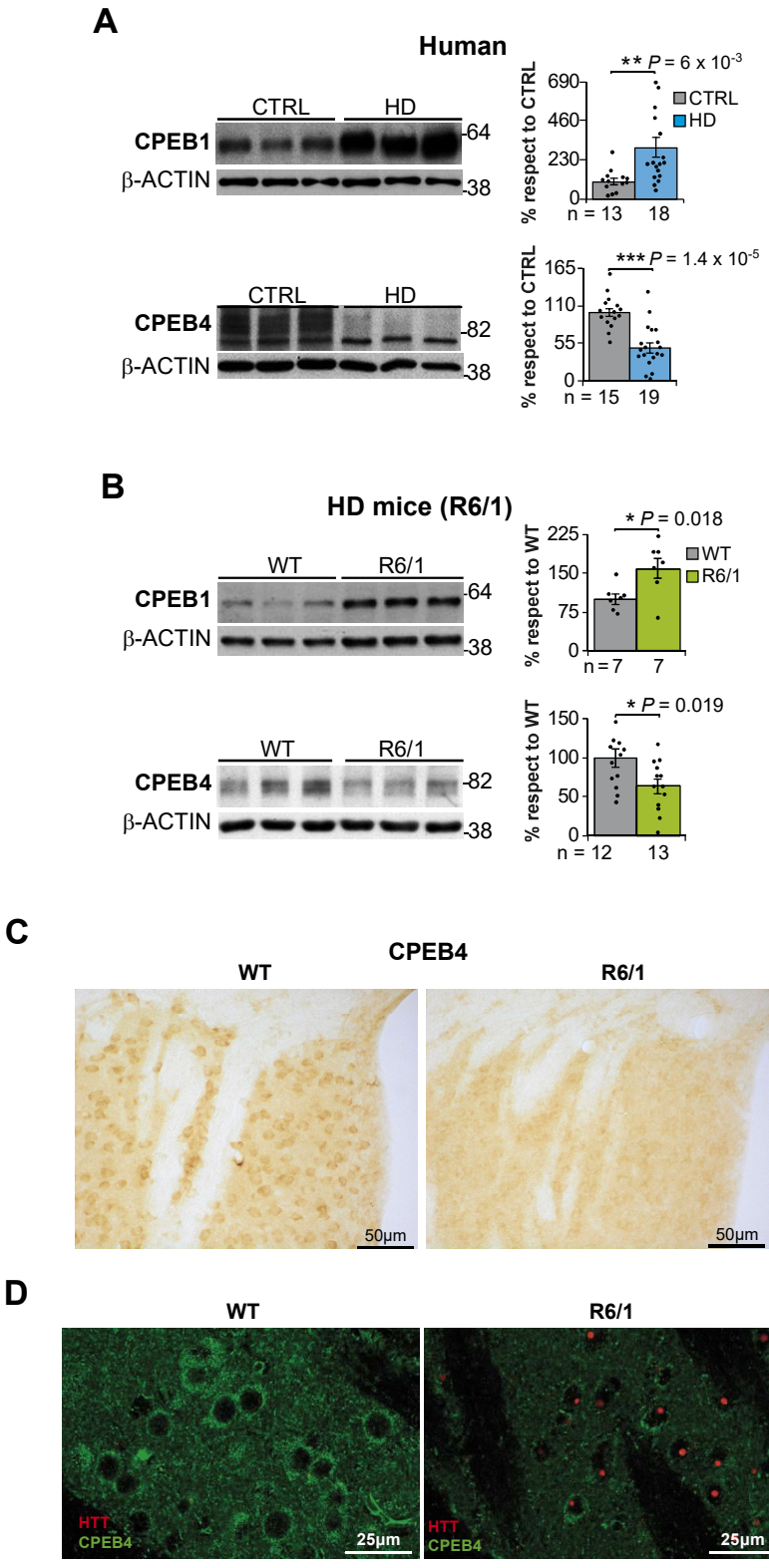

Fig. 1. CPEB1/4 imbalance in HD striatum. (**A**,**B**) CPEB1 and CPEB4 protein levels in (**A**) control or HD striatum, and (**B**) wild-type or R6/1 mice striatum. (**C**) CPEB4 immunohistochemistry in wild-type or R6/1 mice striatum. (**D**) CPEB4 (green) and HTT (red) immunofluorescence in wild-type or R6/1 mice striatum. (A,B) Two-sided unpaired t-test. Graphs show mean ± s.e.m.

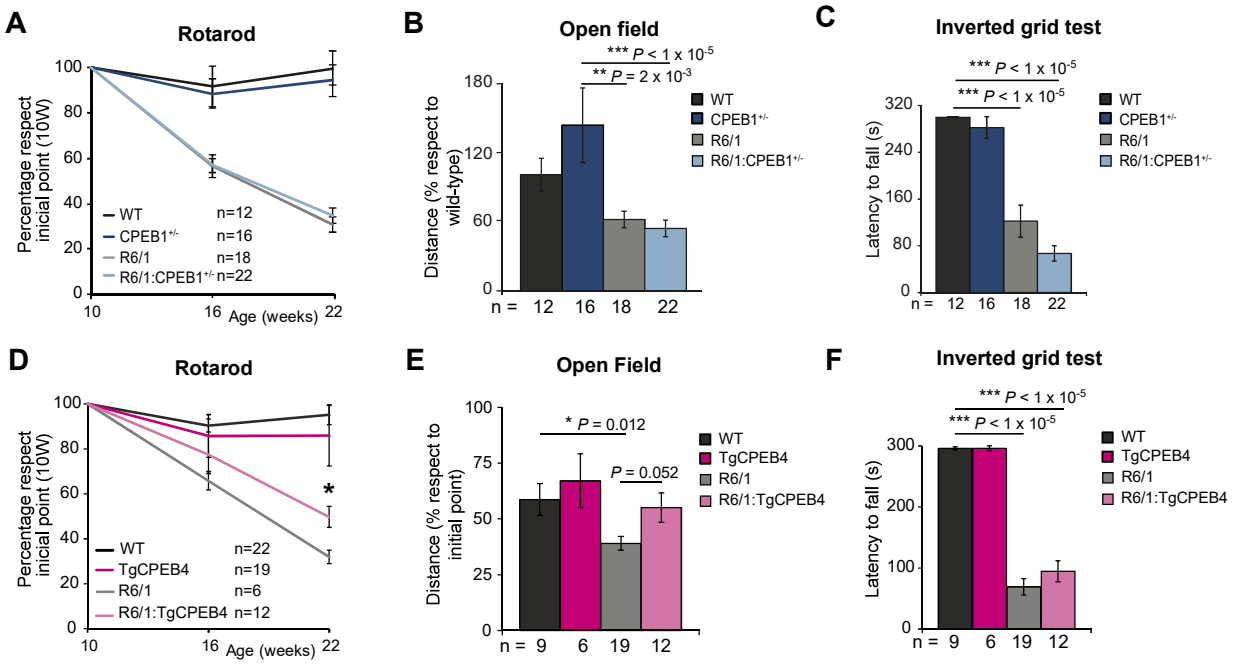

Fig. 2. Attenuation of R6/1 phenotype through CPEB4 overexpression. (**A**, **D**) Latency to fall off the rotarod for (**A**) wild-type, CPEB1+/-, R6/1 or R6/1:CPEB1+/- mice and (**D**) wild-type, TgCPEB4, R6/1 or R6/1:TgCPEB4 mice. (**B**, **E**) Ambulatory distance travelled for (B) wild-type, CPEB1+/-, R6/1 or R6/1:CPEB1+/- mice (22 weeks-old) and (**E**) wild-type, TgCPEB4, R6/1 or R6/1:TgCPEB4 mice (18 weeks-old respect to 10 weeks-old). (**C**, **F**) Latency to fall off the inverted grid test for (**C**) wild-type, CPEB1+/-, R6/1 or R6/1:CPEB1+/- mice (22 weeks-old) and (**F**) wild-type, TgCPEB4, R6/1 or R6/1:TgCPEB4 mice (22 weeks-old). One way-ANOVA followed by Tukey's post-hoc test. Graphs show mean ± s.e.m.

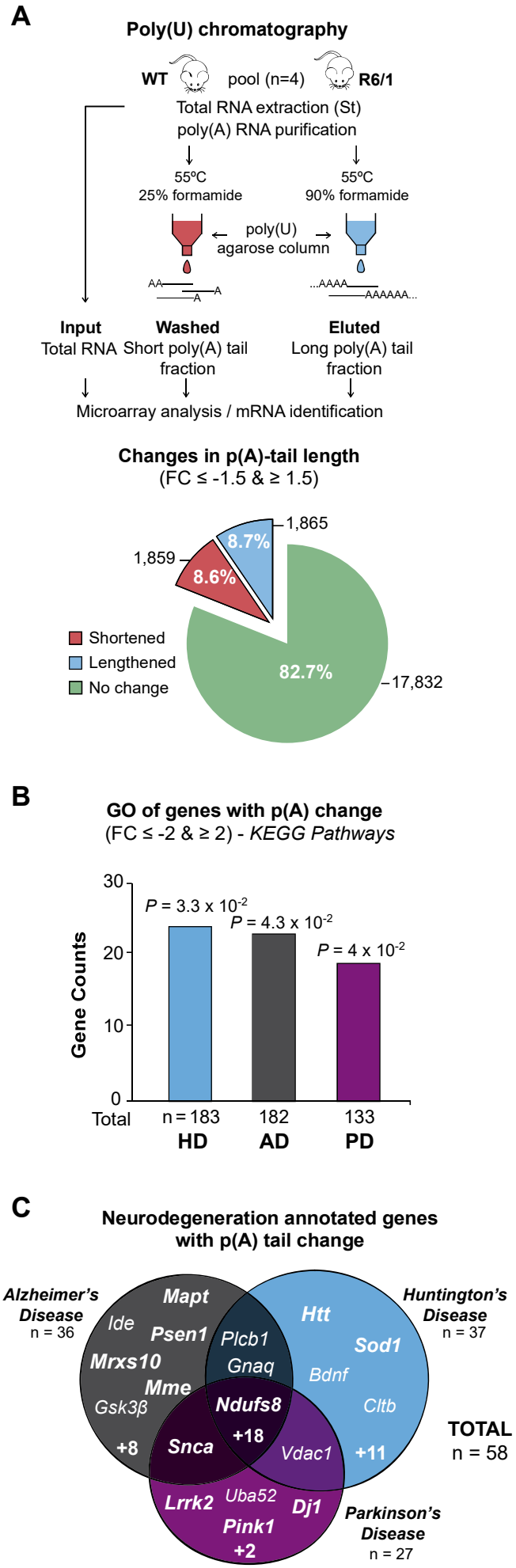

Fig. 3. Global poly(A) alteration in HD affects neurodegeneration related genes. (**A**) Poly(U) chromatography design and percentage of transcripts with lengthened or shortened poly(A) in R6/1 striatum (FC ≤ -1.5 & ≥ 1.5). (**B**) Gene counts from GO analysis of mRNAs with altered poly(A)-tail (FC ≤ -2 & ≥ 2). (**C**) Venn diagram of neurodegenerative disease-related genes with altered poly(A) (FC ≤ -1.5 & ≥ 1.5); Mendelian disease–linked genes are shown in bold. (B) Benjamini–Hochberg corrected P-value.

A

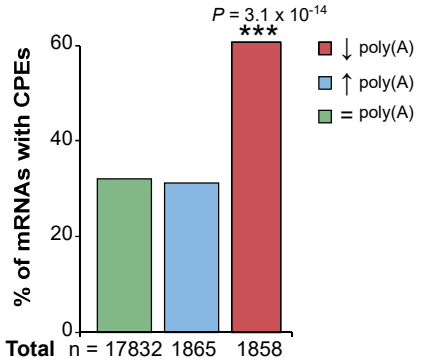

B

Transcripts with shortened p(A)-tail length (FC < -4.0)

FC	Symbol	Gene Name	n. CPEs
-5.4	*Auts2*	Autism susceptibility candidate 2	2
-5.3	*Akap10*	A kinase (PRKA) anchor protein 10	1
-5.0	*Zfp518a*	Zinc finger protein 518A	5
-5.0	*Tcf12*	Transcription factor 12	2
-4.9	*Zw10*	Zw10 kinetochore protein	0
-4.9	*Rock1*	Rho-associated coiled-coil containing protein kinase 1	4
-4.9	*Tmem161b*	Transmembrane protein 161B	3
-4.9	*Spcs1*	Signal peptidase complex subunit 1	2
-4.7	*Lax1*	Lymphocyte transmembrane adaptor 1	1
-4.6	*Memo1*	Mediator of cell motility 1	2
-4.5	*Ktn1*	Kinectin 1	3
-4.3	*Tfrc*	Transferrin receptor	2
-4.2	*Nmd3*	NMD3 homolog (S. cerevisiae)	3
-4.1	*Slc19a3*	Solute carrier family 19, member 3	3

C

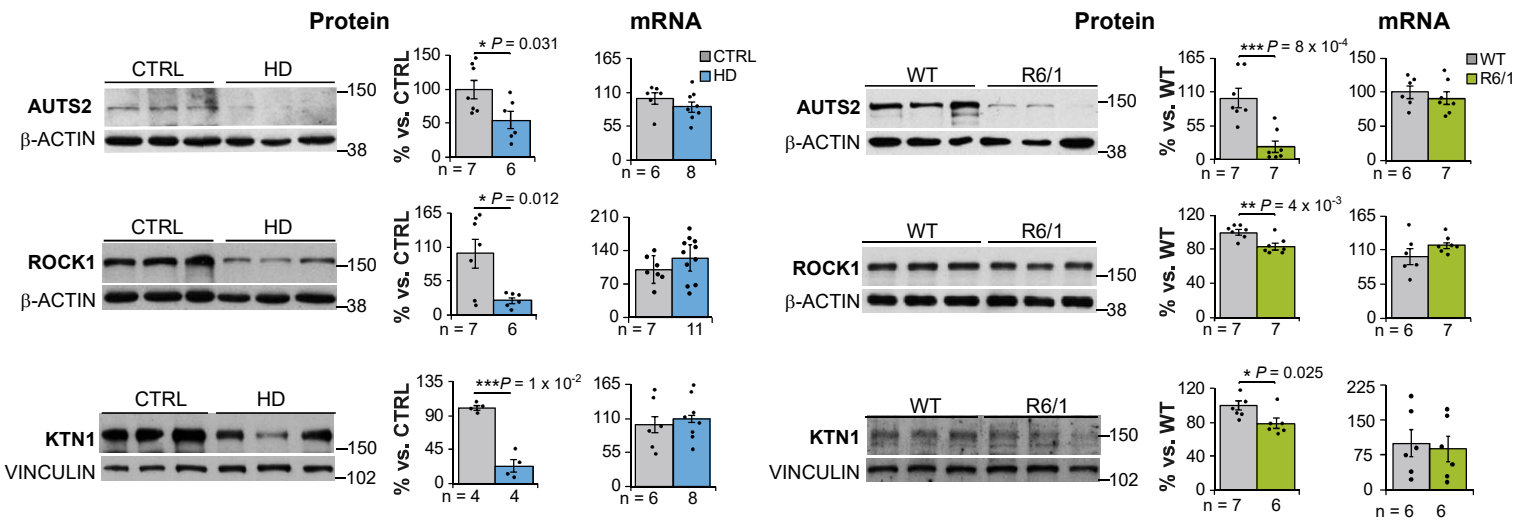

Fig. 4. Top deadenylated transcripts show decreased protein levels. (**A**) Incidence of CPEs in 3'UTR according to the mRNA poly(A) change. (**B**) Symbol, gene name and number of CPEs of most deadenylated transcripts in R6/1 mice. (**C**) AUTS2, ROCK1 and KTN1 protein and mRNA levels in control or HD striatum, and wild-type or R6/1 mouse striatum. (A) One-sided Fisher's exact-test. (C) Two-tailed unpaired t-test. Graphs show mean ± s.e.m.

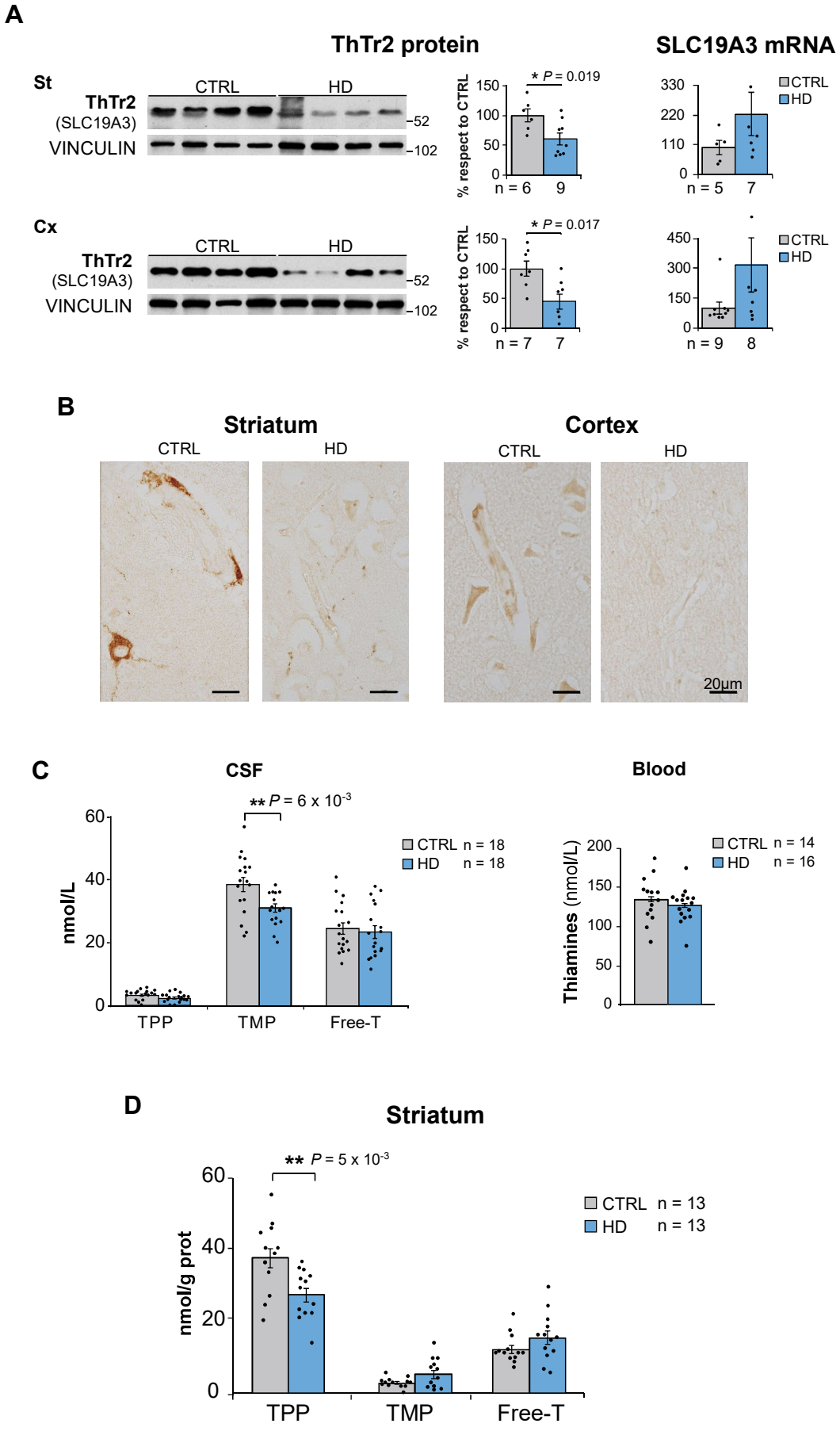

Fig. 5. Decreased ThTr2 and thiamine in HD. (**A**, **B**) SLC19A3 protein (ThTr2) and mRNA levels (**A**) and ThTr2 immunohistochemistry (**B**) in control and HD striatum and cortex. (**C**) Quantification of thiamines in control and HD CSF (nmol/L) and whole-blood (nmol/L). (**D**) Quantification of thiamines in control and HD striatum (nmol/g protein). Two-tailed unpaired t-test. Graphs show mean ± s.e.m.

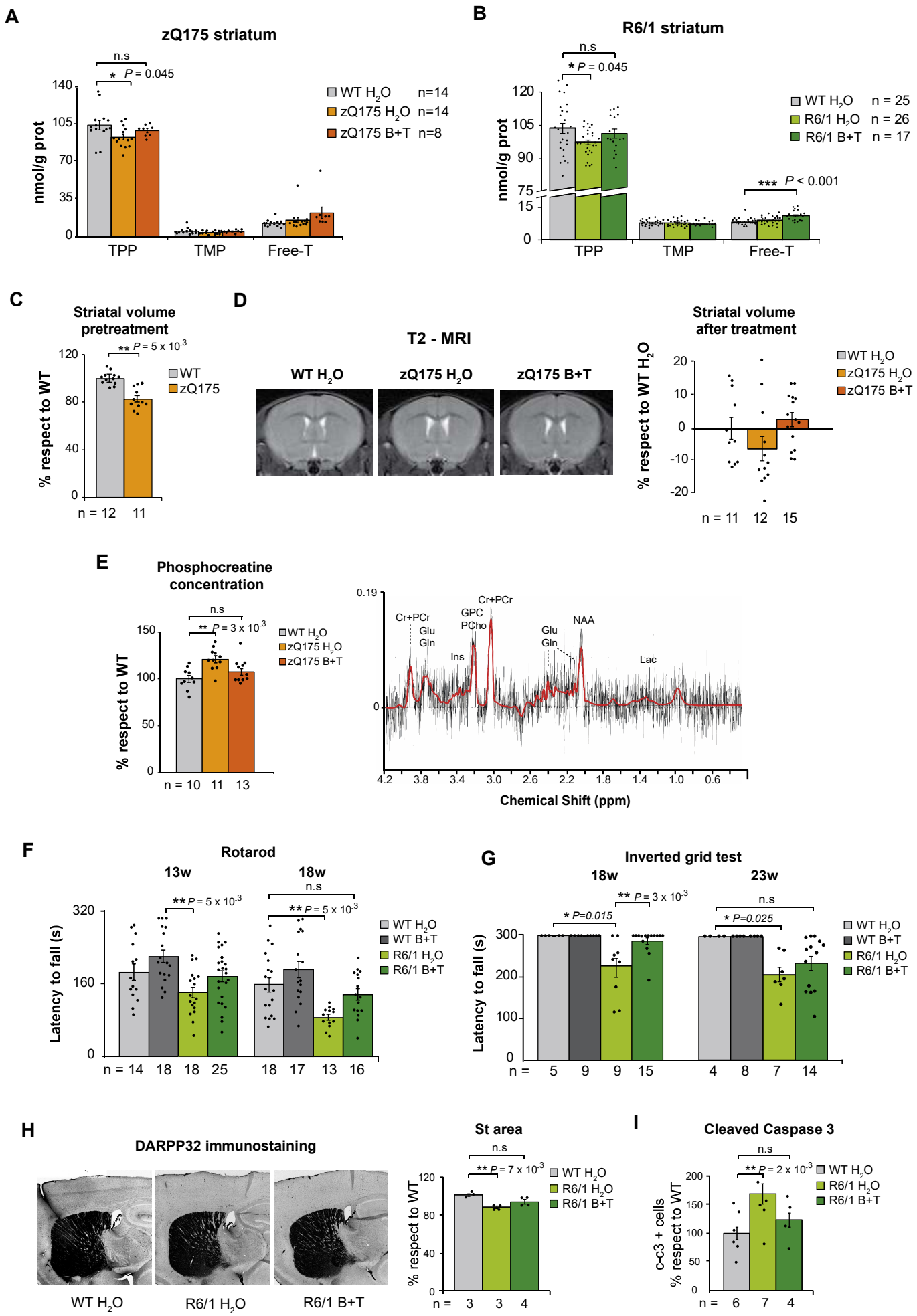

Fig. 6. Attenuation of HD mice phenotype upon biotin+thiamine (B+T). (**A**, **B**) Concentration of thiamines in striatum (nmol/g protein) of (**A**) wild-type or zQ175 mice with or without B+T and (**B**) wild-type or R6/1 mice with or without B+T. (**C**, **D**) In vivo T2-weighted MRI quantification of striatal volume of (**C**) untreated 17 week-old wild type or zQ175 mice and (**D**) treated and untreated 24 week-old wild type or zQ175 mice. (**E**) Phosphocreatine concentration (left) by MR spectroscopy in striatum of wild-type or zQ175 mice with or without B+T (example of spectra on the right). (**F**) Latency to fall off the rotarod for wild-type or R6/1 mice with or without B+T. (**G**) Latency to fall off the inverted grid test for wild-type or R6/1 mice with or without B+T. (**H**) DARPP32-immunostained striatal area in wild-type or R6/1 mice with or without B+T. (I) Quantification of Cleaved-caspase3 positive cells in brain of wild-type or R6/1 mice with or without B+T. (C) Two-tailed unpaired t-test; (A,B,D,E,F,G,H,I) One way-ANOVA followed by Tukey's post-hoc test. Graphs show mean ± s.e.m.

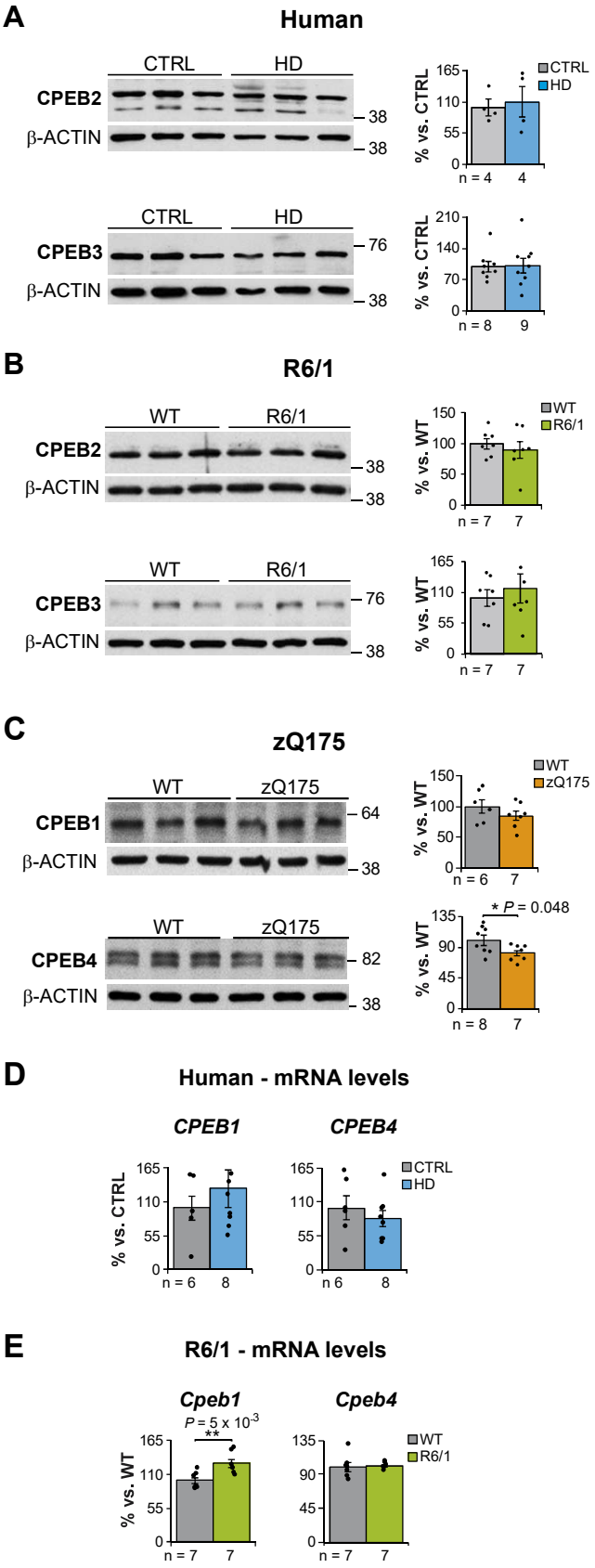

Fig. S1. CPEB status in HD and HD mice. (**A**, **B**) CPEB2 and CPEB3 protein levels in (**A**) control or HD striatum, and (B) wild-type or R6/1 mice striatum. (**C**) CPEB1 and CPEB4 protein levels in wild-type or zQ175 mice striatum. (**D**, **E**) CPEB1 and CPEB4 mRNA levels in (**D**) control or HD striatum, and (**E**) wild-type or R6/1 mice striatum. Two-tailed unpaired t-test. Graphs show mean ± s.e.m.

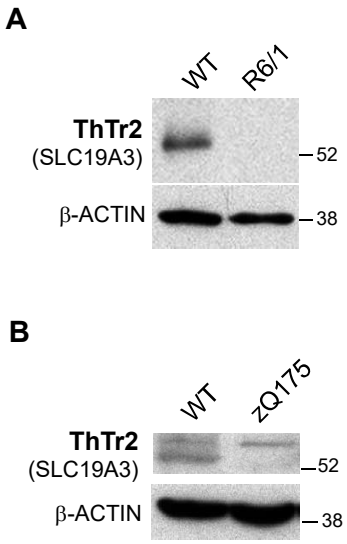

Fig. S2. ThTr2 in HD mice. (**A**, **B**) SLC19A3 protein (ThTr2) levels in (**A**) wild-type or R6/1 mouse and in (**B**) wild-type or zQ175 brain vessels.